

# Path-LLM: A Multi-Modal Path Representation Learning by Aligning and Fusing with Large Language Models

## ABSTRACT

The advancement of intelligent transportation systems has led to a growing demand for accurate path representations, which are essential for tasks such as travel time estimation, path ranking, and trajectory analysis. However, traditional path representation learning (PRL) methods often focus solely on single-modal road network data, overlooking important physical and regional factors that influence real-world traffic dynamics. To overcome this limitation, we introduce **Path-LLM**, a multi-modal path representation learning model that integrates large language models (LLMs) into PRL. Our approach leverages LLMs to interpret both topological and textual data, enabling robust multi-modal path representations. To effectively align and merge these modalities, we propose *TPalign*, a contrastive learning-based pretraining strategy that ensures alignment within the embedding space. We then present *TPfusion*, a multimodal fusion module that dynamically adjusts the weight of each modality before integration. To further optimize LLM training, we introduce a *Two-stage Overlapping Curriculum Learning (TOCL)* approach, which progressively increases the complexity of the training data. Finally, we evaluate Path-LLM on two real-world datasets across traditional PRL downstream tasks, achieving up to a 61.84% improvement in path ranking performance on the Xi’an dataset. Additionally, Path-LLM demonstrates superior performance in both few-shot and zero-shot learning scenarios. Our code is available at: <https://anonymous.4open.science/r/Path-LLM-F053>.

## KEYWORDS

Path representation learning, Large language models, Curriculum learning, Contrastive Learning

## 1 INTRODUCTION

Paths are fundamental to numerous real-world intelligent transportation applications and mapping services, such as travel time estimation [8, 16, 21, 35], path ranking [34, 36, 37], and trajectory analysis [15, 26, 27, 29]. As web-based transportation systems expand in both scale and complexity, the demand for accurate path representations has surged, positioning path representation learning (PRL) a key research focus [11, 38]. PRL aims to generate generalizable representations of paths, enabling their effective use across a diverse range of downstream tasks.

Previous PRL methods [32, 33, 35, 36] predominantly rely on single-modal data, typically focusing on road network graphs that emphasize the connectivity and spatial relationships between road segments. However, a high-quality path representation should incorporate multiple factors, including physical (e.g., road length and width) and functional (e.g., road name and type) characteristics, which capture the essential attributes of paths and are crucial for downstream tasks. For example, as illustrated in Figure 1, there are two potential routes from point  $S$  to  $D$ :  $P_1 = \langle e_1, e_2, e_3, e_4, e_5 \rangle$  and  $P_2 = \langle e_7, e_8, e_6 \rangle$ . While both paths cover similar distances, their differing physical and functional features affect travel efficiency.

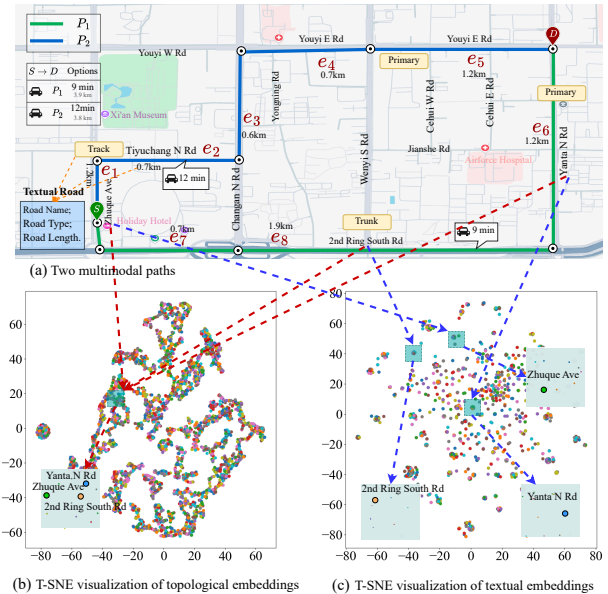


**Figure 1: An Example of Two Paths with Multi-modality Information.** Road segments are described using names, lengths, and types. Road names are often named based on their geographic location, local landmarks, or road type, offering insights into continuity and significance and function. Length helps assess each segment’s importance, while type informs the model about its structural and functional role.

$P_1$ , which traverses ‘2nd Ring South Rd’—a major trunk road with smooth traffic flow and fewer traffic lights—takes just 3 minutes to travel. In contrast,  $P_2$ , which follows ‘Tiyuchang N Rd’ and experiences more interruptions and congestion, takes 10 minutes. Therefore, it is essential to develop a path representation learning method that integrates multimodal information to accurately capture path dynamics.

Recently, large language models (LLMs) have achieved remarkable success in natural language processing (NLP) [2, 6, 7, 19, 30], excelling in both textual and sequential modeling. Given that the physical, regional, and functional information of paths can be expressed in textual form, and that paths can be represented as sequences of road segments—analogueous to sentences—LLMs hold significant potential for advancing path representation learning. LLMs’ advanced NLP capabilities allow them to effectively handle the textual information within paths. Additionally, their strong performance in few-shot and zero-shot tasks demonstrates their ability to learn path representations with high generalization, even in data-scarce scenarios such as regions with limited road data.

117 However, LLMs struggle to model the complex topological struc- 175  
 118 tures inherent in paths, posing two major challenges for PRL, which 176  
 119 are outlined as follows. 177

120 (1) **How can the topological and textual modalities be ef-** 178  
 121 **fectively integrated to ensure the model captures both the** 179  
 122 **spatial structure and semantic features of the paths?** Due to 180  
 123 the differences between these modalities, two consecutive road 181  
 124 segments in a path might be spatially close in the topological em- 182  
 125 bedding space but distant in the textual embedding space. For in- 183  
 126 stance, in Figure 1 (a),  $e_8$  and  $e_6$  denote edges on '2nd Ring South Rd 184  
 127 East Section' and 'Yanta N Rd', respectively, which are close in the 185  
 128 topological embedding space (cf. Figure 1 (b)), yet their textual em- 186  
 129 beddings are far apart (cf. Figure 1 (c)). Thus, it is crucial to develop 187  
 130 an effective fusion mechanism that ensures the complementarity 188  
 131 of topological and textual information. 189

132 (2) **How can LLMs be trained to maintain strong generaliza-** 190  
 133 **tion capabilities despite discrepancies in training difficulties?** 191  
 134 Continuing with the previous point, the degree of discrepancy be- 192  
 135 tween the topological and textual embeddings of different segments 193  
 136 can vary considerably. For example,  $e_1$ ,  $e_8$ , and  $e_6$  are all close in 194  
 137 the topological embedding space (cf. Figure 1 (b)), but the distance 195  
 138 between the textual embeddings of  $e_6$  and  $e_8$  is larger compared 196  
 139 to that between  $e_1$  and  $e_8$  (cf. Figure 1 (c)), making it more chal- 197  
 140 lenging for the model to align topology and textual embeddings. 198  
 141 Therefore, the training process must account for these variations 199  
 142 in alignment difficulty to ensure effective fusion and improve the 200  
 143 model's generalization performance. 201

144 To address these challenges, we propose **Path-LLM**, a multi- 202  
 145 modal path representation learning model that effectively lever- 203  
 146 ages the power of LLMs to integrate both topological and textual 204  
 147 modalities. To address the first challenge, we propose a contrastive 205  
 148 learning-based pretraining strategy, namely *TPalign*, and a multi- 206  
 149 modal fusion module, namely *TPfusion*. To mitigate conflicts be- 207  
 150 tween modalities, *TPalign* is first used to pretrain the path encoder, 208  
 151 aligning topological and textual modalities within the embedding 209  
 152 space, which lays the groundwork for effective multimodal fusion. 210  
 153 To further enhance information complementarity, we design the 211  
 154 *TPfusion* module, which employs an adaptive gating mechanism 212  
 155 to dynamically adjust the weight distribution between modalities, 213  
 156 enabling a more refined integration of topological and textual em- 214  
 157 beddings with precise importance balancing. To address the second 215  
 158 challenge, we propose the **Two-stage Overlapping Curriculum** 216  
 159 **Learning method (TOCL)**, which incorporates two key stages: 1) 217  
 160 *single-step overlapping training* and 2) *two-stage curriculum learn-* 218  
 161 *ing*. The former ensures a smoother transition from easier to more 219  
 162 difficult samples, while the latter helps to prevent catastrophic for- 220  
 163 getting and enhances the model's generalization capabilities. These 221  
 164 two components are particularly crucial in multimodal training, 222  
 165 where alignment discrepancies between modalities can vary sig- 223  
 166 nificantly. Further details will be discussed in Section 4. Our main 224  
 167 contributions are summarized as follows: 225

- 168 • We propose a multimodal path representation learning model 226  
 169 Path-LLM, which uses a partially frozen LLM to interpret the 227  
 170 topological, physical, regional, and functional information 228  
 171 of paths. To the best of our knowledge, this is the first work 229  
 172 that introduces LLMs into path representation learning. 230  
 173 231

- To facilitate multimodal integration, we propose multimodal 175  
 align and fusion modules, i.e., *TPalign* and *TPfusion*, respec- 176  
 tively. Specifically, *TPalign* aims to align the textual and 177  
 topological embeddings, and then *TPfusion* can model the 178  
 interactions between modalities. 179
- To improve the model's generalization capability, we pro- 180  
 pose a two-stage overlapping curriculum learning method 181  
 to prevent catastrophic forgetting. 182
- We conduct extensive experiments on two real-world datasets, 183  
 Xi'an and Chengdu, across two downstream tasks to evaluate 184  
 the performance of Path-LLM. The results demonstrate that 185  
 Path-LLM consistently outperforms the baselines in all tasks, 186  
 showing superior generalization and fusion capabilities. 187  
 188

## 2 RELATED WORK 189

### 2.1 Path Representation Learning 190

191 Path representation learning (PRL) is an important research field 192  
 193 for understanding and predicting patterns in transportation net- 193  
 194 works. Its main goal is to learn universal low-dimensional em- 194  
 195 beddings that capture both road segment attributes and topolog- 195  
 196 ical information. Compared to the specific tasks-oriented meth- 196  
 197 ods [5, 8, 20, 21, 31, 37], PRL can be applied to a variety of down- 197  
 198 stream tasks such as travel time estimation and path ranking. Re- 198  
 199 cently, several in-depth studies [17, 32, 33, 35] have been conducted 199  
 200 on PRL. PIM [32] is an unsupervised learning framework that re- 200  
 201 lies on high-quality negative samples for training path encoders 201  
 202 through mutual information maximization. However, generating 202  
 203 effective negative samples in data-scarce environments remains a 203  
 204 challenge. WSCCL [33] introduces curriculum learning strategies 204  
 205 but suffers from high model complexity and computational cost, 205  
 206 limiting its application to large-scale datasets. LightPath [35] re- 206  
 207 lies on sparse autoencoders and global local knowledge distillation 207  
 208 methods. In comparison, our method simplifies data preparation 208  
 209 and training processes. JGRM [24] presents a trajectory represen- 209  
 210 tation learning framework based on GPS trajectory modality and 210  
 211 topological route modality based on MLM Loss and Match Loss, 211  
 212 respectively. Although methods such as PIM, WSCCL, and Light- 212  
 213 Path focus solely on the topological modality, and while JGRM 213  
 214 incorporates both GPS trajectory and topological modalities, there 214  
 215 is a noticeable gap in the exploration of path representations that 215  
 216 consider both topological and textual modalities. In response to 216  
 217 this, we propose **Path-LLM**, a novel approach that integrates both 217  
 218 topological and textual modalities to learn a more comprehensive 218  
 219 and generic path representation. 219

### 2.2 Cross Domain Application of LLM 220

221 Recent advances in large language models (LLMs) have demon- 221  
 222 strated their potential across various multimodal applications, in- 222  
 223 cluding time series analysis [18, 28, 39] and computer vision tasks [1, 223  
 224 3, 12, 14]. These approaches typically employ domain-specific en- 224  
 225 coders to map data into representations for LLMs, facilitating down- 225  
 226 stream tasks. These methods commonly use domain-specific en- 226  
 227 coders to convert sample data into embeddings for LLMs, aiding 227  
 228 downstream tasks. While the mentioned studies offer valuable in- 228  
 229 sights, their methods are specific to their fields, and cannot be 229  
 230 directly applied to PRL. To our knowledge, no existing research 230  
 231 232

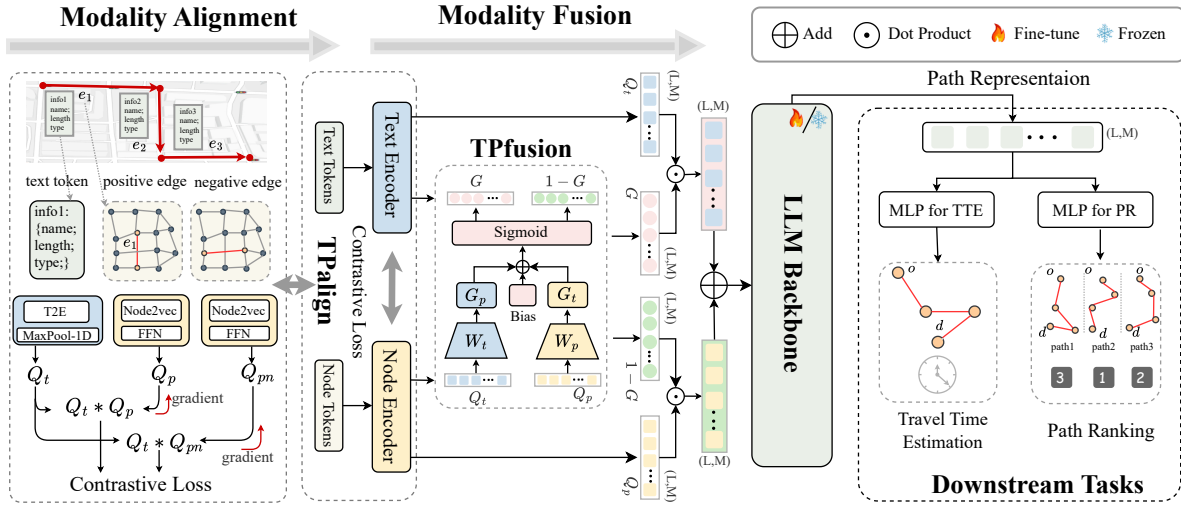


Figure 2: Path-LLM Overview

systematically focuses on applying LLMs to path representation learning.

### 3 PRELIMINARY

In this section, we introduce the basic definitions and concepts required to understand our proposed path representation learning framework, including definitions related to road networks, multi-modal paths, and path representations.

#### 3.1 Basic Definitions

**DEFINITION 1. Road Network.** A road network is represented as a graph  $\mathcal{G} = (V, E)$ , where  $V$  is the set of nodes  $v_i$  representing road intersections, and  $E \subseteq V \times V$  is an edge set, where  $e_i = (v_j, v_k)$  represents a road segment from  $v_j$  to  $v_k$ .

**DEFINITION 2. Topological Path.** A topological path is defined as  $p = \langle e_1, e_2, \dots, e_L \rangle$ , which consists of an ordered sequence of edges, where two consecutive edges  $e_i = (v_i, v_k)$  and  $e_{i+1} = (v_k, v_{i+1}) \in E$  share a common vertex, denoted as  $e_i \cap e_{i+1} = v_k$ , and  $L$  is the length of path  $p$ .

**DEFINITION 3. Textual Path.** Given a topological path  $p$ , a textual path is defined as  $t = \langle a_1, a_2, \dots, a_L \rangle$ , which  $a_i$  denotes the textual description (e.g., road name, type and length, etc.) of edge  $e_i$ .

**DEFINITION 4. Edge Representation.** In a road network graph, the topological representation of an edge is denoted by the embedding  $h_p \in \mathbb{R}^{D_p}$ , which is obtained from graph embedding models such as Node2Vec [10], and the textual representation of an edge is denoted by  $h_t \in \mathbb{R}^{D_t}$  that is obtained by text-embeddings-3<sup>1</sup> from OpenAI.

<sup>1</sup><https://platform.openai.com/docs/guides/embeddings>

#### 3.2 Problem Definitions

In a graph network  $\mathcal{G}$ , the objective of multimodal path representation learning for a path set  $\mathbb{P} = \{p_i, t_i\}_{i=1}^N$  is to learn a function  $F_\theta(\cdot)$  that can generate a generic multi-modal path representation  $O \in \mathbb{R}^M$  for each path  $p \in \mathbb{P}$ , which can be used for the downstream tasks. It can be expressed as follows:

$$O = F_\theta(p, t) : (\mathbb{R}^{L \times D_p}, \mathbb{R}^{L \times D_t}) \rightarrow \mathbb{R}^{L \times M}, \quad (1)$$

where  $O$  is the learned generic multi-modal path representation,  $\theta$  denotes the learnable parameters for the whole model,  $L$  is the length of the input path, and  $M$  is the total number of paths used in the training process.  $D_p$  and  $D_t$  denote the feature dimensions for the edge embeddings for topological and textual path, respectively, and  $M$  is the output dimension for path representation.

### 4 METHODS

This section provides an overview of Path-LLM, which consists of four key components: a pre-trained modality align module (TPalign), a multimodal fusion module (TPfusion), a frozen pre-trained LLM, and a two-stage overlapping curriculum learning model (TOCL), as illustrated in Figures 2 and 4, respectively. The subsequent sections offer detailed descriptions of each component.

#### 4.1 Input Embeddings

Road segments can be characterized by both spatial relationships and textual information. This duality offers complementary insights: topological embeddings elucidate the structural configuration of the road network, while textual embeddings facilitate the interpretation of human-readable information, such as the functions and attributes of specific road segments. The following section will specifically introduce the construction methods for the two types of embeddings.

233  
234  
235  
236  
237  
238  
239  
240  
241  
242  
243  
244  
245  
246  
247  
248  
249  
250  
251  
252  
253  
254  
255  
256  
257  
258  
259  
260  
261  
262  
263  
264  
265  
266  
267  
268  
269  
270  
271  
272  
273  
274  
275  
276  
277  
278  
279  
280  
281  
282  
283  
284  
285  
286  
287  
288  
289  
290

291  
292  
293  
294  
295  
296  
297  
298  
299  
300  
301  
302  
303  
304  
305  
306  
307  
308  
309  
310  
311  
312  
313  
314  
315  
316  
317  
318  
319  
320  
321  
322  
323  
324  
325  
326  
327  
328  
329  
330  
331  
332  
333  
334  
335  
336  
337  
338  
339  
340  
341  
342  
343  
344  
345  
346  
347  
348

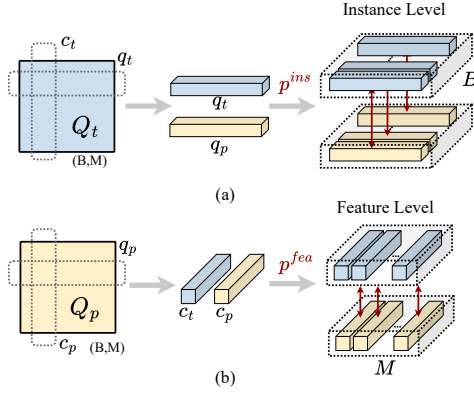


Figure 3: Instance-level CL and Feature-level CL.

**4.1.1 Textual Path Construction.** To capture the key attributes, such as name, type, and length—for each segment in path  $p$ , we introduce LLMs to interpret the textual path. In particular, segment names offer insights into regional road characteristics; length information allows the model to assess the significance of each segment within the overall path. Additionally, road type information aids the model in understanding the functional and structural properties of various road segments, thereby enhancing path representations. We retrieve road segment names, lengths, and types from OpenStreetMap [13]. For a given topological path  $p = \langle e_1, e_2, \dots, e_L \rangle$ , we can obtain the corresponding textual path  $t = \langle a_1, a_2, \dots, a_L \rangle$ , where  $a_i$  represents the textual information of  $e_i$ .

**4.1.2 Modality Embeddings.** As shown in the left-most part of Figure 2, we employ OpenAI’s text-embeddings-3 (T2E) followed by a 1D Max-Pooling layer as the text encoder, while the edge encoder combines Node2Vec [10] with a Feed Forward Network (FFN). We use edge encoder and text encoder to obtain topological embeddings  $Q_p$  and textual embeddings  $Q_t$  for all road segments in a path, respectively, as defined in Equations 2 and 3.

$$H_p = \text{Node2vec}(p); Q_p = \text{FFN}(H_p); \quad (2)$$

$$H_t = \text{T2E}(t); Q_t = \text{MaxPool1D}(H_t), \quad (3)$$

where,  $H_p \in \mathbb{R}^{L \times D_p}$ ,  $H_t \in \mathbb{R}^{L \times D_t}$ ,  $D_p$  and  $D_t$  correspond to the feature dimensions of the path and text respectively.  $Q_p \in \mathbb{R}^{L \times M}$ ,  $Q_t \in \mathbb{R}^{L \times M}$ ,  $M$  represents the input dimension of LLM.

## 4.2 Align and Fuse

The spatial nature of topological information in path limits LLMs’ interpretation compared to textual data. To address it, we propose a multimodal fusion module, TPfusion, which aligns these modalities to enhance their interactions. Specifically, we introduce a contrastive learning-based pretraining module, TPalign, to align topological data with textual information. This alignment is essential for enabling LLMs to interpret path data more meaningfully and spatially awarely.

**4.2.1 Topological and Textual Path Modality Alignment (TPalign).** TPalign performs contrastive learning (CL) tasks at both the instance and feature levels to pretrain the Feed Forward Network (FFN)

of the edge encoder, as shown in Figure 3. At the instance level, it aligns the textual and topological embeddings of individual road segments, which focuses on minimizing the distance between textual embeddings and their corresponding topological embeddings for the same path, while maximizing the difference between embeddings of different paths. This design ensures that LLMs can better understand and utilize the spatial context in path representations. At the feature level, it aligns the embeddings across feature dimensions to facilitate TPfusion better integrating multimodal information across different feature dimensions.

Specifically, given a road segment  $e_i \in E$ , we denote the positive embeddings as  $h_t^i$  and  $h_p^i$ , and negative embeddings as  $h_t^j$  and  $h_p^j$ , where  $i \neq j$ . Our goal is to bring the positive pair closer in the embedding space and push the negative pair further apart.

In *instance-level CL*, we construct positive/negative pairs as  $(q_t^i, q_p^i)$  and  $(q_t^j, q_p^j)$ , where  $q_p^i = \text{FFN}(h_p^i)$  and  $q_t^i = \text{Maxpool1D}(h_t^i)$ . Then, the similarity of one pair embedding can be calculated as follows.

$$S(q_p^m, q_t^n) = \text{Sigmoid}(\text{MLP}(q_p^m || q_t^n)), \quad (4)$$

where  $S(q_p^m, q_t^n)$  denotes the similarity function that measures the similarity of a pair of topological and textual path embeddings of two edges,  $e_m$  and  $e_n$ , respectively.  $||$  denotes the concatenation operation, and  $\text{Sigmoid}(\cdot)$  denotes the Sigmoid function.

Let  $y$  represent the label of pair embeddings, where positive pairs are assigned a value of 1 and negative pairs are assigned a value of 0. Then, we construct a set of training data as  $\mathbb{B} = \{(\hat{q}_p^i, \hat{q}_t^i, y^i)\}$ . Then, we calculate the instance-level contrastive loss as follows:

$$\mathcal{L}_{\text{ins}} = -\frac{1}{|\mathbb{B}|} \sum_{i=1}^{|\mathbb{B}|} [y^i \log S(\hat{q}_p^i, \hat{q}_t^i) + (1 - y^i) \log \log S(\hat{q}_p^i, \hat{q}_t^i)]. \quad (5)$$

In *feature-level CL*, we treat the textual embeddings corresponding to all road segments in each batch as a textual feature matrix  $Q_t \in \mathbb{R}^{B \times M}$ . Similar to the instance-level, we can obtain a positive feature matrix  $Q_p^+$  and the negative  $Q_p^-$ , where  $Q_p = [q_p^i]_{i=1}^B \in \mathbb{R}^{B \times M}$ . The column embeddings of matrices  $Q_t$  and  $Q_p$  are represented as  $c_t$  and  $c_p$  respectively. For the  $j$ -th pair  $(c_t^j, c_p^j)$  within  $M$  columns, we compute the similarity as:

$$H(c_p^m, c_t^n) = \text{Sigmoid}(\text{MLP}(c_p^m || c_t^n)), \quad (6)$$

where  $H(c_p^m, c_t^n)$  denotes the similarity function that measures the similarity of a pair of topological and textual path embeddings of two columns,  $c_m$  and  $c_n$ , respectively.

Let  $z$  represent the label of pair embeddings, where the positive column pair is assigned a value of 1 and the negative pair is assigned a value of 0. Then, we construct a set of training data as  $\mathbb{M} = \{(\hat{c}_p^i, \hat{c}_t^i, z^i)\}$ . The feature-level contrastive loss is computed as:

$$\mathcal{L}_{\text{fea}} = -\frac{1}{|\mathbb{M}|} \sum_{i=1}^{|\mathbb{M}|} [z^i \log H(\hat{c}_p^i, \hat{c}_t^i) + (1 - z^i) \log \log H(\hat{c}_p^i, \hat{c}_t^i)]. \quad (7)$$

Finally, the overall training loss is computed as a weighted combination of the instance-level and feature-level losses:

$$\mathcal{L} = \lambda \mathcal{L}_{\text{ins}} + (1 - \lambda) \mathcal{L}_{\text{fea}}, \quad (8)$$

where  $\lambda$  is a hyperparameter that balances the contributions of the instance-level and feature-level contrastive losses.

465 **4.2.2 Topological and Textual Path Modality Fusion (TPfusion).** To  
 466 improve the effective parsing of multimodal information by LLMs,  
 467 it is necessary to fuse these two features. However, directly adding  
 468 the textual and topological features or applying static weights may  
 469 lead to conflicts between the modalities. To address this issue, we  
 470 propose a multimodal fusion module, TPfusion, which dynamically  
 471 adjusts the contribution of each modality by selectively weighting  
 472 different positions. Specifically, the topological and textual embed-  
 473 dings  $Q_p$  and  $Q_t$  are fed into a gated fusion module to compute a  
 474 gate value  $G \in \mathbb{R}^{L \times M}$  based on the linear transformations of both  
 475 input features, followed by a sigmoid activation function:

$$476 \quad G = \text{Sigmoid}(W_p Q_p + W_t Q_t + b), \quad (9)$$

477 where  $W_p \in \mathbb{R}^{L \times M}$  and  $W_t \in \mathbb{R}^{L \times M}$  are learnable weight matrices,  
 478  $b \in \mathbb{R}^M$  is the bias term. The sigmoid function ensures that the gate  
 479 values range between 0 and 1. The final fused representation  $Q_f$  is  
 480 obtained by combining  $Q_p$  and  $Q_t$  using the computed gate values,  
 481 where the gate values control the contribution of each modality:

$$482 \quad Q_f = G \odot Q_p + (1 - G) \odot Q_t, \quad (10)$$

483 where  $\odot$  denotes the element-wise multiplication operator.

### 484 **4.3 Pre-Trained and Frozen LLM Block.**

485 We employ a pre-trained GPT-2 model [19] to enhance path rep-  
 486 resentation learning, capitalizing on its efficacy in sequential data  
 487 processing. To maximize its embedded knowledge while minimiz-  
 488 ing computational costs, we utilize a selective fine-tuning strategy,  
 489 as inspired by [39].

490 **4.3.1 Freezing Layers:** During the training phase, we freeze both  
 491 the multi-head self-attention (MHA) and feed-forward network  
 492 (FFN) layers in GPT-2. These components have already been trained  
 493 to capture general patterns from large-scale language data, and  
 494 freezing them prevents overfitting to the current task, while also  
 495 reducing the training time and computational complexity. By freez-  
 496 ing these layers, we retain the robust representational power of the  
 497 pre-trained GPT-2 model.

498 **4.3.2 Fine-tuning Positional Embeddings and Layer Normalization:**  
 499 To enable the model to adapt to path representation learning, we  
 500 fine-tune specific layers that can better capture task-specific infor-  
 501 mation. First, we fine-tune the word positional embeddings (WPE),  
 502 allowing the model to better encode the sequential nature of paths.  
 503 Paths inherently exhibit spatial and topological structures, which  
 504 positional embeddings can effectively represent by learning the  
 505 relative positions of road segments. Furthermore, we fine-tune the  
 506 layer normalization (LN) layers to stabilize training and enhance  
 507 model performance, ensuring that gradient updates remain stable  
 508 during transformations.

509 **4.3.3 Skipping Input Embeddings:** We bypass the original input  
 510 embedding layer in GPT-2 and use the fused representation  $Q_f$   
 511 from TPfusion as the direct input, then we obtain a universal path  
 512 representation  $O \in \mathbb{R}^{L \times M}$ .

513 2024-10-15 12:24. Page 5 of 1–9.

## 514 **4.4 Two-stage OverLapping Curriculum Learning**

515 Fine-tuning large language models (LLMs) for specific tasks, par-  
 516 ticularly when integrating multiple modalities, poses a significant  
 517 challenge in maintaining generalization capabilities. Traditional  
 518 fine-tuning approaches often lead to overfitting on task-specific  
 519 data, reducing the model’s ability to generalize across diverse sce-  
 520 narios. Additionally, when handling complex multimodal data, the  
 521 model may struggle to effectively balance the learning of both  
 522 simple and complex examples, further impairing performance. To  
 523 address these issues, we propose Two-stage OverLapping Curricu-  
 524 lum Learning, termed as TOCL. The overview of TOCL is illustrated  
 525 in Figure 4.

526 **4.4.1 Single Step Overlapping Training:** In this phase, TOCL adopts  
 527 a progressive learning strategy, where the model  $\theta_i$  is trained incre-  
 528 mentally over  $N$  rounds, with each round introducing increasingly  
 529 complex data. Unlike traditional methods, TOCL selects the train-  
 530 ing data for each round using a sliding window approach, ensuring  
 531 that each round’s data partially overlaps with the previous round’s  
 532 data. This overlap allows the model to reinforce previously acquired  
 533 knowledge while progressively integrating more challenging data.

534 The training data is ranked by Mean Squared Error (MSE), sorting  
 535 paths from the easiest to the most challenging. For each round  $i$ ,  
 536 a window of size  $\gamma_i$  is defined, with start and end indices denoted  
 537 by  $x_i^{st}$  and  $x_i^{end}$  respectively. This approach ensures that the model  
 538 encounters only simpler data in the early stages and progressively  
 539 introduces more complex data as training advances. The data from  
 540 round  $i$  partially overlaps with the data from round  $i-1$ . This design  
 541 aims to allow the model to review previously learned knowledge  
 542 in each training round, thereby ensuring a smooth transition to  
 543 learning more complex data.

544 **4.4.2 Two-Stage Curriculum:** TOCL further introduces a two-stage  
 545 training strategy to balance both complex and fundamental knowl-  
 546 edge retention. As illustrated in Figure 4, this process is divided  
 547 into two phases: (1) Stage 1 (Round 1 to  $K$ ): In the first  $K$  rounds,  
 548 the model is progressively trained on all data using the single-step  
 549 overlapping approach. This phase allows the model to build a strong  
 550 foundation by gradually increasing the complexity of the training  
 551 data; (2) Stage 2 (Rounds  $K+1$  to  $N$ ): From round  $K+1$  to round  
 552  $N$ , the model is trained on all data again. This ensures that the  
 553 model not only retains and understands complex knowledge but  
 554 also consolidates basic knowledge.

## 555 **5 EXPERIMENTS**

### 556 **5.1 Datasets and Settings**

557 We conduct experiments on real-world datasets from the cities of  
 558 Chengdu and Xi’an. The original datasets, released by Didi, consist  
 559 of GPS trajectories recorded by taxis in the two cities. We obtain  
 560 the urban road networks from OpenStreetMap to perform map-  
 561 matching on the trajectories. We remove paths shorter than 10  
 562 segments. Ultimately, the Chengdu dataset contains 4,315 road  
 563 segments and 121,526 paths, while the Xi’an dataset includes 3,392  
 564 road segments and 94,917 paths.

525  
526  
527  
528  
529  
530  
531  
532  
533  
534  
535  
536  
537  
538  
539  
540  
541  
542  
543  
544  
545  
546  
547  
548  
549  
550  
551  
552  
553  
554  
555  
556  
557  
558  
559  
560  
561  
562  
563  
564  
565  
566  
567  
568  
569  
570  
571  
572  
573  
574  
575  
576  
577  
578  
579  
580

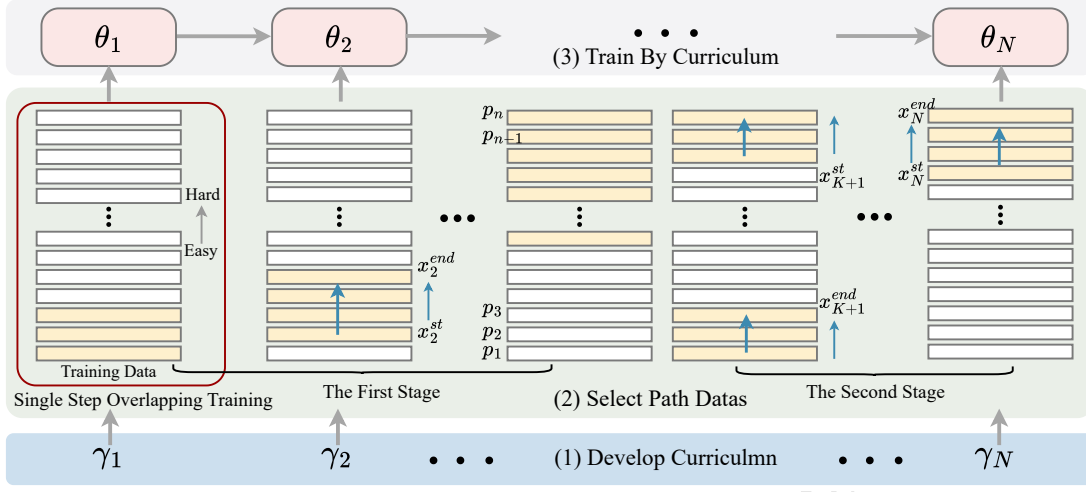


Figure 4: The Training Process of TOCL

We divide each city’s dataset into training, testing, and validation sets with a ratio of 8:1:1. We use GPT-2 as the base LLM for development, and all models are implemented using PyTorch [25]. We set the training process to 40 epochs. All experiments are conducted on Linux server with an NVIDIA RTX3090 24GB GPU. Our code is available at: <https://anonymous.4open.science/r/Path-LLM-F053>.

## 5.2 Downstream Tasks

In our study, we conduct experimental analysis on two downstream tasks:

**Travel Time Estimation (TTE):** We extract the travel time for each path from the original trajectory data. We make predictions using a fully connected layer, as described below:

$$\hat{y}_{TTE} = FC_{TTE}(O). \quad (11)$$

To evaluate the performance of TTE, we use Mean Absolute Error (MAE) [33], Mean Absolute Percentage Error (MAPE) [33] and Mean Absolute Relative Error (MARE) [33]. Lower values of these metrics indicate better performance.

**Path Ranking:** We consider the path used by drivers in historical trajectories as the optimal path. Then, for each optimal path, we generate multiple candidate paths connecting the same origin and destination using path finding algorithm [23]. Finally, we calculate the Jaccard similarity coefficient between the optimal path and each candidate path to determine the ranking score:

$$J(A, B) = \frac{|A \cap B|}{|A \cup B|}, \quad (12)$$

where  $A$  and  $B$  represent two sets, while  $|A \cap B|$  and  $|A \cup B|$  denotes the size of their intersection and union, respectively. Similar to TTE, we use a fully connected layer to predict the ranking score. In addition to MAE, we also use the Kendall rank correlation coefficient ( $\tau$ ), and Spearman’s rank correlation coefficient ( $\rho$ ) as metrics for path ranking evaluation:

$$\tau = \frac{N_{con} - N_{dis}}{n(n-1)/2}, \quad (13)$$

$$\rho = 1 - \frac{6 \sum_{i=1}^n d_i^2}{n(n^2 - 1)/2}, \quad (14)$$

where  $N_{con}$  and  $N_{dis}$  represent the number of concordant and discordant pairs in the two rankings, respectively. In Equation 14,  $d_i$  represents the difference in rank for the  $i$ -th path in both rankings. For instance, if the true rank of  $p_i$  is 1 and the predicted rank is 3, then  $d_i = 1 - 3 = -2$ .

## 5.3 Baselines

We compare with 8 path representation learning baselines. The details of methods are described as follows:

- **Node2vec** [10] is a graph embedding algorithm designed to learn continuous representations of nodes in a graph, effectively capturing both structural roles and community affiliations.
- **Toast** [4] is a road network representation framework that obtains effective road segment representations through traffic context aware skip-gram module and trajectory-enhanced transformer module.
- **PIM** [32] is an unsupervised path representation learning method that first employs curriculum learning to generate negative samples, followed by leveraging both global and local mutual information maximization to learn effective path representations.
- **Trembr** [9] is a representation learning framework based on a recurrent neural network, which incorporates the Road2Vec model to learn road segment embeddings.
- **PathRank** [36] is a supervised path representation learning method that employs Gated Recurrent Units (GRU) to model path sequences.
- **HMTRL** [22] utilizes a spatiotemporal graph neural network to capture autocorrelation and employs an attention module to generate route representations.
- **START** [17] is a self-supervised framework that utilizes a Graph Attention Network to convert road network features into segment embeddings.

**Table 1: Overall accuracy in travel time estimation and path ranking tasks. We use ‘ $\uparrow$ ’ (and ‘ $\downarrow$ ’) to indicate that larger (and smaller) values are better. For each task, we highlight the best and second-best performance in bold and underline. “Improvement” quantifies the enhancements achieved by Path-LLM over the best baseline.**

Method	Xi’an						Chengdu					
	Travel Time Estimation			Path Ranking			Travel Time Estimation			Path Ranking		
	MAE $\downarrow$	MARE $\downarrow$	MAPE $\downarrow$	MAE $\downarrow$	$\tau$ $\uparrow$	$\rho$ $\uparrow$	MAE $\downarrow$	MARE $\downarrow$	MAPE $\downarrow$	MAE $\downarrow$	$\tau$ $\uparrow$	$\rho$ $\uparrow$
Node2vec	5.926	0.300	34.801	0.175	0.551	0.614	4.539	0.309	38.367	0.28	0.519	0.571
Toast	5.786	0.295	33.742	0.180	0.629	0.672	6.151	0.424	61.585	0.320	0.394	0.415
PIM	4.512	0.228	24.892	0.143	0.664	0.737	3.450	0.241	27.934	0.192	0.570	0.628
Trembr	4.814	0.247	29.505	0.089	0.676	0.747	4.211	0.299	35.598	<u>0.149</u>	0.666	0.735
PathRank	4.696	0.234	25.735	0.155	0.667	0.735	3.610	0.255	30.854	<u>0.231</u>	0.618	0.674
HMTRL	4.516	0.228	25.786	0.164	0.676	0.749	3.557	0.246	28.897	0.259	0.653	0.721
START	4.642	0.234	26.313	0.116	0.682	0.753	3.328	0.229	26.237	0.231	<u>0.671</u>	<u>0.739</u>
LightPath	<u>4.424</u>	<u>0.223</u>	<u>24.346</u>	<u>0.076</u>	<u>0.693</u>	<u>0.760</u>	<u>3.304</u>	<u>0.225</u>	<u>26.142</u>	0.204	0.560	0.627
<b>Path-LLM</b>	<b>4.179</b>	<b>0.207</b>	<b>20.885</b>	<b>0.029</b>	<b>0.766</b>	<b>0.819</b>	<b>3.096</b>	<b>0.213</b>	<b>23.290</b>	<b>0.093</b>	<b>0.706</b>	<b>0.772</b>
Improvement	5.86%	7.17%	14.22%	61.84%	10.55%	7.76%	6.30%	5.33%	10.91%	37.58%	4.96%	4.27%

- **LightPath** [35] is a scalable and lightweight path representation learning framework based on sparse path encoder and relational reasoning.

## 5.4 Results and Analysis

**5.4.1 Overall Performance.** Table 1 presents the performance comparison of Path-LLM with all baseline models across two datasets under two downstream tasks. Overall, Path-LLM outperforms all the baselines in both datasets and across all evaluation metrics, demonstrating the superiority of our model. Specifically, we make the following observations.

Node2Vec performs poorly on downstream tasks across both datasets due to its limitations of graph embedding methods in capturing spatial relationships along a path. Both Toast and PathRank utilize bidirectional Gated Recurrent Unit (GRU) to capture sequential information. However, since Toast is primarily designed for trajectory representation learning, its architecture is more focused on modeling movement patterns. PIM relies on the construction of high-quality negative samples for their effectiveness, which results in the performance instability across different datasets and tasks. The performance of Trembr and HMTRL demonstrate the advantages of sequence modeling approaches in handling long sequence data. LightPath and START both employ contrastive learning approaches, and their performance surpasses that of most baseline models, indicating the significant advantage of contrastive learning in capturing distinctive features for path representation. However, their reliance solely on the road network topology modality may constrain their performance in complex paths. In contrast, Path-LLM integrates multi-modal information of paths, enabling a multifaceted understanding of paths that enhances the richness and accuracy of path representations, as well as improving performance across various tasks.

**5.4.2 Zero-shot Travel Time Estimation.** To evaluate the transferability of Path-LLM across different cities, we conduct the following zero-shot travel time estimation experiments: (1) Chengdu  $\rightarrow$  Xi’an: the model is trained on the Chengdu dataset and evaluated

on the Xi’an dataset; (2) Xi’an  $\rightarrow$  Chengdu: the model is trained on the Xi’an dataset and evaluated on the Chengdu dataset. These experiments aim to evaluate the generalization capability of Path-LLM on unseen datasets, particularly in cross-city scenarios where variations in the physical characteristics and regional features of paths may impact the model’s performance. From the results in Table 2, it is evident that Path-LLM demonstrates significantly superior zero-shot performance compared to other baseline models.

**5.4.3 Few-shot Travel Time Estimation.** Evaluating the few-shot learning capability of Path-LLM under data-scarce conditions is also a key focus of our study. To simulate such scenarios, we conduct few-shot time estimation experiments on the Xi’an and Chengdu datasets, using 5% and 30% of the data samples, respectively, as shown in Table 3 and Table 4. The results show that Path-LLM exhibits robust generalization ability, even when the training data is extremely limited.

**5.4.4 Ablation Studies.** To evaluate the contribution of each component in Path-LLM, we conduct a comparative analysis between the full model and several variants:

- w/o Topology: This variant excludes the topological modality, relying only on the textual modality.
- w/o Text: This variant omits the textual modality, and uses only the topological modality as input.
- w/o TPFusion: This variant replaces the multimodal fusion module TPFusion with a linear layer.
- w/o TPAIalign: This variant removes the TPAIalign task, retaining only the TPFusion module.
- w/o TOCL: This variant randomly splits the dataset, and trains the model using randomly sampled batches.

We measure the performance of these variants across the Xi’an dataset on TTE and PR tasks, and the results are presented in Table 5. Based on the results, we make the following observations: (1) The variant w/o Topology significantly reduces performance, emphasizing the importance of topological information in both PR and TTE tasks; (2) The variant w/o Text also leads to performance

**Table 2: Zero-shot learning in TTE task.**

Methods	Path-LLM			LightPath			START			PathRank			Trembr			HMTRL		
Metric	MAE	MARE	MAPE	MAE	MARE	MAPE	MAE	MARE	MAPE	MAE	MARE	MAPE	MAE	MARE	MAPE	MAE	MARE	MAPE
Chengdu → Xi'an	<b>7.412</b>	<b>0.363</b>	<b>34.890</b>	9.810	0.557	73.057	9.730	0.473	44.425	9.983	0.479	43.602	12.518	0.616	53.885	10.594	0.550	84.841
Xi'an → Chengdu	<b>5.116</b>	<b>0.359</b>	<b>42.251</b>	<u>6.474</u>	<u>0.424</u>	45.175	8.801	0.625	78.613	7.289	0.473	<u>42.797</u>	7.896	0.573	74.545	7.071	0.460	45.548

**Table 3: Few-shot learning in TTE task on 5% label data.**

Methods	Path-LLM			LightPath			START			PathRank			Trembr			HMTRL		
Metric	MAE	MARE	MAPE	MAE	MARE	MAPE	MAE	MARE	MAPE	MAE	MARE	MAPE	MAE	MARE	MAPE	MAE	MARE	MAPE
Chengdu	<b>3.649</b>	<b>0.251</b>	<b>29.705</b>	<u>3.387</u>	<u>0.259</u>	30.793	4.170	0.291	36.331	4.662	0.304	30.692	4.983	0.357	43.500	4.607	0.299	<u>28.983</u>
Xi'an	<b>4.481</b>	<b>0.222</b>	<b>23.265</b>	<u>4.807</u>	<u>0.241</u>	<u>26.955</u>	5.515	0.278	31.651	7.160	0.381	49.656	6.164	0.294	29.746	7.357	0.395	52.901

**Table 4: Few-shot learning in TTE task on 30% label data.**

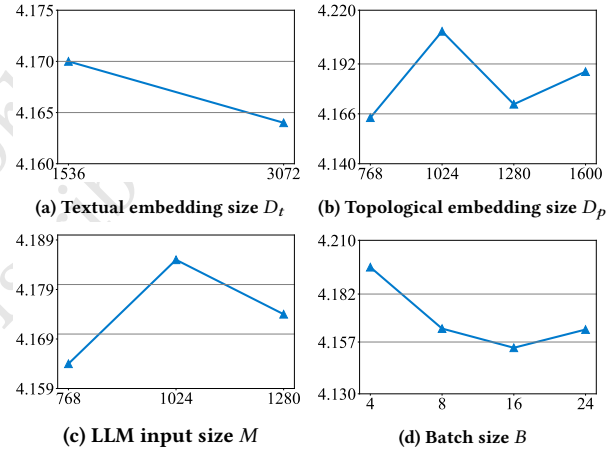
Methods	Path-LLM			LightPath			START			PathRank			Trembr			HMTRL		
Metric	MAE	MARE	MAPE	MAE	MARE	MAPE	MAE	MARE	MAPE	MAE	MARE	MAPE	MAE	MARE	MAPE	MAE	MARE	MAPE
Chengdu	<b>3.292</b>	<b>0.227</b>	<b>25.987</b>	<u>3.387</u>	<u>0.234</u>	25.966	3.527	0.243	28.026	3.514	0.242	27.523	3.894	0.255	24.746	3.648	0.251	29.234
Xi'an	<b>4.332</b>	<b>0.218</b>	<b>23.651</b>	<u>4.584</u>	<u>0.230</u>	<u>25.435</u>	4.799	0.256	28.825	6.131	0.302	30.626	5.080	0.276	31.187	4.880	0.254	28.145

**Table 5: Performance of Variants of Path-LLM**

Methods	Travel Time Estimation			Path Ranking		
	MAE	MARE	MAPE	MAE	$\tau$	$\rho$
w/o Topology	4.418	0.222	24.135	0.032	0.699	0.752
w/o Text	4.304	0.217	22.559	0.032	0.720	0.788
w/o TPfusion	4.519	0.226	24.449	0.030	0.716	0.787
w/o TPalgn	4.226	0.212	22.025	0.032	0.729	0.793
w/o TOCL	4.238	0.213	22.756	0.030	0.723	0.789
<b>Path-LLM</b>	<b>4.179</b>	<b>0.207</b>	<b>20.885</b>	<b>0.029</b>	<b>0.766</b>	<b>0.819</b>

degradation, demonstrating the value of textual data in providing semantic insights and effectively leveraging pre-trained models for prior knowledge utilization; (3) The variant w/o TPfusion significantly reduces the performance of TTE predictions, highlighting the critical role of the TPfusion module in achieving effective multimodal data fusion. Additionally, The variant w/o TPalgn results in performance declines, indicating that proper alignment between textual and topological embeddings is essential for maximizing the effectiveness of TPfusion in multimodal integration; (4) The variant w/o TOCL causes substantial degradation, showcasing the advantages of gradual learning for understanding multimodal path sequences.

**5.4.5 Impact of Hyper-parameters.** In this section, we explore how different hyper-parameters affect the performance of Path-LLM. Specifically, we evaluate the effects of textual embedding size  $D_t$ , topological embedding size  $D_p$ , LLM input embedding size  $M$  and batch size  $B$ . Figure 5 presents the MAE results from the TTE task using Xi'an dataset. Similar trends are observed for the other tasks evaluated. The results indicate that increasing the text embedding size from 1536 to 3072 leads to a decline performance, and a topological embeddings size of  $D_p$  achieves the best results. Increasing the LLM input embeddings results in performance degradation, likely due to the increased parameter count which makes fine-tuning more challenging. When the batch size  $B$  is increased from 4 to 8, the MAE decreases significantly, but further increases offer only

**Figure 5: Effects of hyper-parameters.**

marginal improvements. Therefore, setting  $B = 8$  is the optimal choice when computational resources are limited.

## 6 CONCLUSIONS

In this work, we propose Path-LLM, a novel multi-modal path representation learning model that utilizes LLMs to integrate the topological, physical, regional, and functional characteristics of paths. We propose *TPalign*, a contrastive pretraining strategy to reduce modal conflicts by aligning multimodal embeddings. We also design *TPfusion* that dynamically adjusts modality importance. To train LLMs effectively, we introduce *TOCL*, a curriculum learning approach that gradually increases data complexity. Extensive experiments demonstrate the superior performance of Path-LLM. In the future, we aim to further explore multi-modal representation techniques for paths to achieve more comprehensive representations, which are critical for intelligent transportation systems.

## REFERENCES

- [1] Hangbo Bao, Li Dong, Songhao Piao, and Furu Wei. 2021. Beit: Bert pre-training of image transformers. *arXiv preprint arXiv:2106.08254* (2021).
- [2] Tom Brown, Benjamin Mann, Nick Ryder, Melanie Subbiah, Jared D Kaplan, Prafulla Dhariwal, Arvind Neelakantan, Pranav Shyam, Girish Sastry, Amanda Askell, et al. 2020. Language models are few-shot learners. In *NeurIPS*, Vol. 33. 1877–1901.
- [3] Gongwei Chen, Leyang Shen, Rui Shao, Xiang Deng, and Liqiang Nie. 2024. Lion: Empowering multimodal large language model with dual-level visual knowledge. In *CVPR*. 26540–26550.
- [4] Yile Chen, Xiucheng Li, Gao Cong, Zhifeng Bao, Cheng Long, Yiding Liu, Arun Kumar Chandran, and Richard Ellison. 2021. Robust road network representation learning: When traffic patterns meet traveling semantics. In *CIKM*. 211–220.
- [5] Zebin Chen, Xiaolin Xiao, Yue-Jiao Gong, Jun Fang, Nan Ma, Hua Chai, and Zhiguang Cao. 2022. Interpreting Trajectories from Multiple Views: A Hierarchical Self-Attention Network for Estimating the Time of Arrival. In *KDD*. 2771–2779.
- [6] Jacob Devlin, Ming-Wei Chang, Kenton Lee, and Kristina Toutanova. 2018. Bert: Pre-training of deep bidirectional transformers for language understanding. *arXiv preprint arXiv:1810.04805* (2018).
- [7] Zhengxiao Du, Yujie Qian, Xiao Liu, Ming Ding, Jiezhong Qiu, Zhilin Yang, and Jie Tang. 2021. Glm: General language model pretraining with autoregressive blank infilling. *arXiv preprint arXiv:2103.10360* (2021).
- [8] Kun Fu, Fanlin Meng, Jieping Ye, and Zheng Wang. 2020. CompactETA: A fast inference system for travel time prediction. In *SIGKDD*. 3337–3345.
- [9] Tao-Yang Fu and Wang-Chien Lee. 2020. Trembr: Exploring road networks for trajectory representation learning. *ACM Transactions on Intelligent Systems and Technology (TIST)* 11, 1 (2020), 1–25.
- [10] Aditya Grover and Jure Leskovec. 2016. node2vec: Scalable feature learning for networks. In *SIGKDD*. 855–864.
- [11] Chenjuan Guo, Bin Yang, Jilin Hu, and Christian Jensen. 2018. Learning to route with sparse trajectory sets. In *ICDE*. 1073–1084.
- [12] Tanmay Gupta, Amita Kamath, Aniruddha Kembhavi, and Derek Hoiem. 2022. Towards general purpose vision systems: An end-to-end task-agnostic vision-language architecture. In *CVPR*. 16399–16409.
- [13] Mordechai Haklay and Patrick Weber. 2008. Openstreetmap: User-generated street maps. *IEEE Pervasive computing* 7, 4 (2008), 12–18.
- [14] Jiaming Han, Kaixiong Gong, Yiyuan Zhang, Jiaqi Wang, Kaipeng Zhang, Dahua Lin, Yu Qiao, Peng Gao, and Xiangyu Yue. 2024. Onellm: One framework to align all modalities with language. In *CVPR*. 26584–26595.
- [15] Xiaolin Han, Reynold Cheng, Chenhao Ma, and Tobias Grubenmann. 2022. DeepTEA: Effective and Efficient Online Time-dependent Trajectory Outlier Detection. In *VLDB*, Vol. 15. 1493–1505.
- [16] Jilin Hu, Bin Yang, Chenjuan Guo, Christian S Jensen, and Hui Xiong. 2020. Stochastic origin-destination matrix forecasting using dual-stage graph convolutional, recurrent neural networks. In *ICDE*. 1417–1428.
- [17] Jiawei Jiang, Dayan Pan, Houxing Ren, Xiaohan Jiang, Chao Li, and Jingyuan Wang. 2023. Self-supervised trajectory representation learning with temporal regularities and travel semantics. In *ICDE*. 843–855.
- [18] Ming Jin, Shiyu Wang, Lintao Ma, Zhixuan Chu, James Y Zhang, Xiaoming Shi, Pin-Yu Chen, Yuxuan Liang, Yuan-Fang Li, Shirui Pan, et al. 2023. Time-llm: Time series forecasting by reprogramming large language models. *arXiv preprint arXiv:2310.01728* (2023).
- [19] Klemens Lagler, Michael Schindelegger, Johannes Böhm, Hana Krásná, and Tobias Nilsson. 2013. GPT2: Empirical slant delay model for radio space geodetic techniques. *Geophysical research letters* 40, 6 (2013), 1069–1073.
- [20] Cheng Li, Jiaqi Ma, Xiaoxiao Guo, and Qiaozhu Mei. 2017. Deepcas: An end-to-end predictor of information cascades. In *WWW*. 577–586.
- [21] Xiucheng Li, Gao Cong, Aixin Sun, and Yun Cheng. 2019. Learning Travel Time Distributions with Deep Generative Model. In *WWW*. 1017–1027.
- [22] Hao Liu, Jindong Han, Yanjie Fu, Jingbo Zhou, Xinjiang Lu, and Hui Xiong. 2020. Multi-modal transportation recommendation with unified route representation learning. In *VLDB*, Vol. 14. 342–350.
- [23] Huiping Liu, Cheqing Jin, Bin Yang, and Aoying Zhou. 2018. Finding Top-k Shortest Paths with Diversity. *IEEE Trans. Knowl. Data Eng.* 30, 3 (2018), 488–502.
- [24] Zhipeng Ma, Zheyuan Tu, Xinhai Chen, Yan Zhang, Deguo Xia, Guyue Zhou, Yilun Chen, Yu Zheng, and Jiangtao Gong. 2024. More Than Routing: Joint GPS and Route Modeling for Refine Trajectory Representation Learning. In *WWW*. 3064–3075.
- [25] Adam Paszke, Sam Gross, Francisco Massa, Adam Lerer, James Bradbury, Gregory Chanan, Trevor Killeen, Zeming Lin, Natalia Gimelshein, Luca Antiga, et al. 2019. Pytorch: An imperative style, high-performance deep learning library. In *NeurIPS*, Vol. 32.
- [26] Zeyuan Shang, Guoliang Li, and Zhifeng Bao. 2018. DITA: A Distributed In-Memory Trajectory Analytics System. In *SIGMOD*. 1681–1684.
- [27] Zeyuan Shang, Guoliang Li, and Zhifeng Bao. 2018. DITA: Distributed In-Memory Trajectory Analytics. In *SIGMOD*. 725–740.
- [28] Chenxi Sun, Yaliang Li, Hongyan Li, and Shenda Hong. 2023. TEST: Text prototype aligned embedding to activate LLM’s ability for time series. *arXiv preprint arXiv:2308.08241* (2023).
- [29] Ruijie Tian, Weishi Zhang, Fei Wang, Kemal Polat, and Fayadh Alenezi. 2023. Tinba: Incremental partitioning for efficient trajectory analytics. *Adv. Eng. Informatics* 57 (2023), 102064.
- [30] Hugo Touvron, Thibaut Lavril, Gautier Izacard, Xavier Martinet, Marie-Anne Lachaux, Timothée Lacroix, Baptiste Rozière, Naman Goyal, Eric Hambro, Faisal Azhar, et al. 2023. Llama: Open and efficient foundation language models. *arXiv preprint arXiv:2302.13971* (2023).
- [31] Chen Xu, Qiang Wang, and Lijun Sun. 2024. Link Representation Learning for Probabilistic Travel Time Estimation. *arXiv preprint arXiv:2407.05895* (2024).
- [32] Sean Bin Yang, Chenjuan Guo, Jilin Hu, Jian Tang, and Bin Yang. 2021. Unsupervised Path Representation Learning with Curriculum Negative Sampling. In *IJCAI*. 3286–3292.
- [33] Sean Bin Yang, Chenjuan Guo, Jilin Hu, Bin Yang, Jian Tang, and Christian S Jensen. 2022. Weakly-supervised temporal path representation learning with contrastive curriculum learning. In *ICDE*. 2873–2885.
- [34] Sean Bin Yang, Chenjuan Guo, and Bin Yang. 2022. Context-Aware Path Ranking in Road Networks. *IEEE Trans. Knowl. Data Eng.* 34, 7 (2022), 3153–3168.
- [35] Sean Bin Yang, Jilin Hu, Chenjuan Guo, Bin Yang, and Christian S. Jensen. 2023. LightPath: Lightweight and Scalable Path Representation Learning. In *SIGKDD*. 2999–3010.
- [36] Sean Bin Yang and Bin Yang. 2019. PathRank: A Multi-Task Learning Framework to Rank Paths in Spatial Networks. *CoRR abs/1907.04028* (2019).
- [37] Sean Bin Yang and Bin Yang. 2020. Learning to rank paths in spatial networks. In *ICDE*. 2006–2009.
- [38] Junbo Zhang, Yu Zheng, Junkai Sun, and Dekang Qi. 2019. Flow prediction in spatio-temporal networks based on multitask deep learning. *IEEE Trans. Knowl. Data Eng.* 32, 3 (2019), 468–478.
- [39] Tian Zhou, Peisong Niu, Liang Sun, Rong Jin, et al. 2023. One fits all: Power general time series analysis by pretrained lm. In *NeurIPS*, Vol. 36. 43322–43355.